



Iodomethane oxidative addition and CO migratory insertion in monocarbonylphosphine complexes of the type $[\text{Rh}((\text{C}_6\text{H}_5)\text{COCHCO}((\text{CH}_2)_n\text{CH}_3))(\text{CO})(\text{PPh}_3)]$: Steric and electronic effects

Nomampondomise F. Stuurman, Jeanet Conradie *

Department of Chemistry, University of the Free State, Nelson Mandela, Bloemfontein 9301, South Africa

ARTICLE INFO

Article history:

Received 19 April 2008

Received in revised form 17 October 2008

Accepted 22 October 2008

Available online 30 October 2008

Keywords:

β -Diketone

Rhodium

Oxidative addition

$\text{p}K_a$

Carbonyl

Phosphine

ABSTRACT

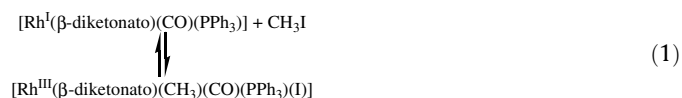
The chemical kinetics, studied by UV/Vis, IR and NMR, of the oxidative addition of iodomethane to $[\text{Rh}((\text{C}_6\text{H}_5)\text{COCHCOR})(\text{CO})(\text{PPh}_3)]$, with $\text{R} = (\text{CH}_2)_n\text{CH}_3$, $n = 1-3$, consists of three consecutive reaction steps that involves isomers of two distinctly different classes of Rh^{III} -alkyl and two distinctly different classes of Rh^{III} -acyl species. Kinetic studies on the first oxidative addition step of $[\text{Rh}((\text{C}_6\text{H}_5)\text{COCHCOR})(\text{CO})(\text{PPh}_3)] + \text{CH}_3\text{I}$ to form $[\text{Rh}((\text{C}_6\text{H}_5)\text{COCHCOR})(\text{CH}_3)(\text{CO})(\text{PPh}_3)(\text{I})]$ revealed a second order oxidative addition rate constant approximately 500–600 times faster than that observed for the Monsanto catalyst $[\text{Rh}(\text{CO})_2\text{I}_2]^-$. The reaction rate of the first oxidative addition step in chloroform was not influenced by the increasing alkyl chain length of the R group on the β -diketonato ligand: $k_1 = 0.0333$ ($[\text{Rh}((\text{C}_6\text{H}_5)\text{COCHCO}(\text{CH}_2\text{CH}_3))(\text{CO})(\text{PPh}_3)]$), 0.0437 ($[\text{Rh}((\text{C}_6\text{H}_5)\text{COCHCO}(\text{CH}_2\text{CH}_2\text{CH}_3))(\text{CO})(\text{PPh}_3)]$) and $0.0354 \text{ dm}^3 \text{ mol}^{-1} \text{ s}^{-1}$ ($[\text{Rh}((\text{C}_6\text{H}_5)\text{COCHCO}(\text{CH}_2\text{CH}_2\text{CH}_2\text{CH}_3))(\text{CO})(\text{PPh}_3)]$). The $\text{p}K_a'$ and keto–enol equilibrium constant, K_c , of the β -diketonates $(\text{C}_6\text{H}_5)\text{COCH}_2\text{COR}$, along with apparent group electronegativities, χ_R of the R group of the β -diketonates $(\text{C}_6\text{H}_5)\text{COCH}_2\text{COR}$, give a measurement of the electron donating character of the coordinating β -diketonato ligand: (R, $\text{p}K_a'$, K_c , χ_R) = (CH_3 , 8.70, 12.1, 2.34), (CH_2CH_3 , 9.33, 8.2, 2.31), ($\text{CH}_2\text{CH}_2\text{CH}_3$, 9.23, 11.5, 2.41) and ($\text{CH}_2\text{CH}_2\text{CH}_2\text{CH}_3$, 9.33, 11.6, 2.22).

© 2008 Elsevier B.V. All rights reserved.

1. Introduction

Rhodium complex compounds are one of the most widely spread industrial homogeneous catalysts for organic raw material processing. Classic examples of efficacious catalyst systems are methanol carbonylation to give acetic acid in the presence of $[\text{Rh}(\text{CO})_2\text{I}_2]$ (Monsato process) [1], alkene hydroformylation by the $[\text{RhHCO}(\text{PPh}_3)_2]$ catalyst [2], hydrogenation of olefins and acetylenes with the help of $[\text{RhCl}(\text{PPh}_3)_3]$ (Wilkinson's catalyst) [3] and the use of $[\text{Rh}(\text{CH}_3\text{COCHCOCH}_3)(\text{CO})_2]$ in the hydroformylation of olefins [4]. In the field of olefin polymerization, metal complexes with a coordinatively unsaturated Lewis acid metal center are generally required, whereas for transformations such as the carbonylation of methanol, electron-rich metal centers are necessary to favor oxidative addition of iodomethane to Rh^{I} [5,6]. High catalytic reactivity of these rhodium complexes is in many respects due to the nature of ligand surroundings [7]. It is of interest to note how the steric and electronic properties of the ancillary ligands can affect the rates of the oxidative addition and migratory insertion steps, which is a vital step in the functioning of many of these compounds as homogeneous catalysts.

The reactivity of square planar rhodium(I) monocarbonylphosphine complexes $[\text{Rh}(\beta\text{-diketonato})(\text{CO})(\text{PPh}_3)]$ in the oxidative addition Reaction (1) with iodomethane was studied with regard to the phosphine basicity [8], the electronic effect of different substituents R' and R on the β -diketonato ligand = $\text{R}'\text{COCHCOR}^-$ [9] and the solvent polarity and donicity effects [10].



Steric factors are important in controlling the rate of oxidative addition reactions [11]. Previous studies on $[\text{Rh}(\beta\text{-diketonato})(\text{CO})(\text{PPh}_3)]$ complexes did not focus on the steric influence of the R or R' groups of the β -diketonato ligand $\text{R}'\text{COCHCOR}^-$ on the reactivity of Reaction (1). In this paper, we report the synthesis and characterization of monocarbonylphosphine complexes $[\text{Rh}((\text{C}_6\text{H}_5)\text{COCHCO}((\text{CH}_2)_n\text{CH}_3))(\text{CO})(\text{PPh}_3)]$, $n = 1-3$, and the oxidative addition reactions of these complexes with iodomethane.

It is found that the electron donating (electronic) properties of the phenyl and alkyl groups on the β -diketonato ligand $\text{R}'\text{COCHCOR}^-$ speed up the oxidative addition reaction, but the size of the alkyl group $(\text{CH}_2)_n\text{CH}_3$ (steric property) did not restrain the rate of oxidative addition. The rate of iodomethane oxidative addition

* Corresponding author. Tel.: +27 51 4012194; fax: +27 51 4446384.
E-mail address: conradj.sci@ufs.ac.za (J. Conradie).

to the complexes of this study was found to be faster than all previously published values according to Reaction (1).

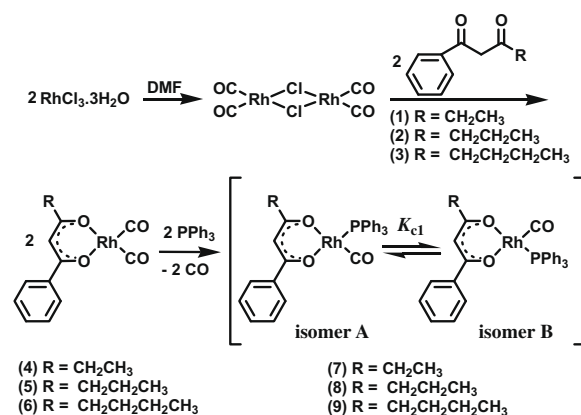
2. Results and discussion

2.1. Synthesis and identification of complexes

The route utilized to obtain the β -diketones of general formula $(\text{C}_6\text{H}_5)\text{COCH}_2\text{COR}$, $\text{R} = (\text{CH}_2)_n\text{CH}_3$, $n = 1-3$, is given in Scheme 1. β -Diketones exist in solution and in gas phase as mixtures of keto and enol tautomers. In the solid state, the enol form is often the form mostly observed [12]. From a ^1H NMR study, by comparing the relative intensities of the CH_2 (keto at *ca* 4.1 ppm) and CH (enol at *ca* 6.2 ppm) signals in solution, the percentage of the keto tautomers in CDCl_3 solution at 25 °C of the β -diketones Hba ($\text{R} = \text{CH}_3$), Hbab (**1**) ($\text{R} = \text{CH}_2\text{CH}_3$), Hbab (**2**) ($\text{R} = \text{CH}_2\text{CH}_2\text{CH}_3$) and Hbav (**3**) ($\text{R} = \text{CH}_2\text{CH}_2\text{CH}_2\text{CH}_3$) was established as 7.5%, 10.9%, 8.0% and 7.9%, respectively. The $\text{p}K_a$ values obtained for the conjugated keto–enol system of the different phenyl-containing β -diketones **1**, **2** and **3** are 9.33(3), 9.23(5) and 9.33(5), respectively. The basic character of these ligands should increase the electron density at the rhodium center, making it a stronger nucleophile and therefore more reactive towards oxidative addition [13].

It has previously been shown that accurate apparent group electronegativities, χ_R , of the R group for esters of the type $\text{R}(\text{C}=\text{O})(\text{OCH}_3)$ can be obtained from a linear fit between χ_R and the IR carbonyl stretching frequency [14]. The straight line generated by the fit of χ_R and $\nu(\text{C}=\text{O})$ (see Fig. S1 in Supplementary material) fits the equation $\nu(\text{C}=\text{O})_R = 74.53 \chi_R + 1561$ and was used to determine the effective or apparent group electronegativities of the R groups = CH_3 , CH_2CH_3 , $\text{CH}_2\text{CH}_2\text{CH}_3$ and $\text{CH}_2\text{CH}_2\text{CH}_2\text{CH}_3$ as 2.34 [15], 2.31, 2.41 and 2.22, respectively. These electronegativities are considered to be electron-donating ($\chi_{\text{CF}_3} = 3.31$) [15], making the β -diketonates **1–3** a good choice to be complexed to rhodium in order to increase the electron density at the metal. The increased electron density at the rhodium center should promote oxidative addition and consequently the overall rate of production during catalytic processes.

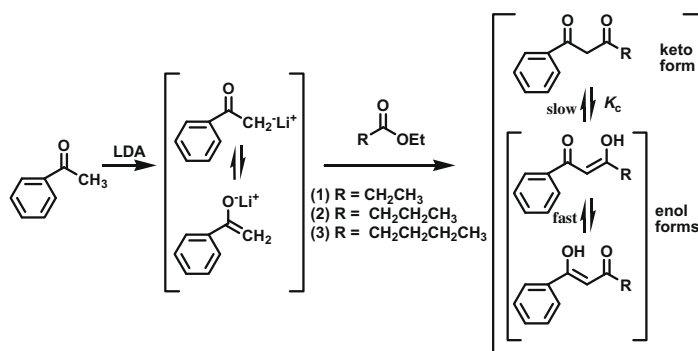
The new yellow-orange complexes of $[\text{Rh}(\beta\text{-diketonato})(\text{CO})_2]$ with β -diketonato = bap (**4**) (27% yield), bab (**5**) (17% yield) and bav (**6**) (18% yield) and the new light yellow $[\text{Rh}(\beta\text{-diketonato})(\text{CO})(\text{PPh}_3)]$ complexes with β -diketonato = bap (**7**) (16% yield), bab (**8**) (13% yield) and bav (**9**) (14% yield) were synthesized as shown in Scheme 2. ^1H NMR spectra showed that for each of the $[\text{Rh}(\beta\text{-diketonato})(\text{CO})(\text{PPh}_3)]$ complexes synthesized, two isomers exist in solution (see Fig. S2 in Supplementary material). The difference between the two isomers is manifested especially in the big



Scheme 2. Synthetic route for the synthesis of $[\text{Rh}(\beta\text{-diketonato})(\text{CO})_2]$ complexes **4–6** and $[\text{Rh}(\beta\text{-diketonato})(\text{CO})(\text{PPh}_3)]$ complexes **7–9** from $\text{RhCl}_3 \cdot 3\text{H}_2\text{O}$ and appropriate β -diketones **1–3**.

difference in the position, δ_{H} in ppm, of the signals of the protons of the alkyl group of the β -diketonato ligand. The two isomers are the isomer with the PPh_3 group *trans* to the oxygen nearest to the more electron donating phenyl group of the chelate ring and the isomer with the PPh_3 group *cis* to the oxygen nearest to the phenyl group. The former is labeled as isomer A and the latter as isomer B, as defined in Scheme 2. Isomer A is expected to be the predominant isomer due to the *trans*-influence where the PPh_3 group is *trans* to the oxygen near an electron donating group (phenyl) which has a larger *trans*-influence compared to an alkyl group. This is in agreement with the polarization theory, since the oxygen atom nearest to an alkyl group will be least polarisable due to the electron attracting property of the alkyl group [16].

The equilibrium constant, defined as $K_c = [\text{isomer B}]/[\text{isomer A}]$ and applicable to the equilibrium shown in Scheme 2, may be determined by calculating the ratio of peak integral values of non-overlapping corresponding signals of each isomer and averaging all answers. $\Delta_r H$ values in CDCl_3 at 25 °C for the $[\text{Rh}(\beta\text{-diketonato})(\text{CO})(\text{PPh}_3)]$ complexes **7–9** were determined with Eq. (15) and are summarized in Table 1, together with the K_c values and the thermodynamic data. (see Fig. S3 in Supplementary material for the variation of K_c with temperature for **7**, **8** and **9**). The enthalpy effect of the interconversion of the $[\text{Rh}(\beta\text{-diketonato})(\text{CO})(\text{PPh}_3)]$ isomers of **7–9**, is smaller than was found for $[\text{Rh}(\beta\text{-diketonato})(\text{CO})(\text{PPh}_3)]$ complexes with β -diketones containing a ferrocenyl group [17] or a thienyl group [18].



Scheme 1. Synthetic route for the synthesis of phenyl containing β -diketones Hbab (1-phenylpentane-1,3-dione, propanylacetophenone, $\text{C}_6\text{H}_5\text{COCH}_2\text{COCH}_2\text{CH}_3$) (**1**), Hbab (1-phenylhexane-1,3-dione, buterylacetophenone, $\text{C}_6\text{H}_5\text{COCH}_2\text{COCH}_2\text{CH}_2\text{CH}_3$) (**2**) and Hbav (1-phenylheptane-1,3-dione, valerylacetophenone, $\text{C}_6\text{H}_5\text{COCH}_2\text{COCH}_2\text{CH}_2\text{CH}_2\text{CH}_3$) (**3**). The keto–enol equilibrium of the β -diketones is indicated on the right.

Table 1

The equilibrium constant K_c in $CDCl_3$ at 25 °C and for the equilibrium shown in Scheme 2 and the thermodynamic data relevant to this equilibrium for $[Rh(ba)(CO)(PPh_3)]$, $[Rh(bap)(CO)(PPh_3)]$ (**7**), $[Rh(bab)(CO)(PPh_3)]$ (**8**) and $[Rh(bav)(CO)(PPh_3)]$ (**9**).

Complex	K_c^a	$\Delta_r H$ (kJ mol ⁻¹)	$\Delta_r G^a$ (kJ mol ⁻¹)	$\Delta_r S$ (J mol ⁻¹ K ⁻¹)
$[Rh(ba)(CO)(PPh_3)]$	0.47	–	–	–
$[Rh(bap)(CO)(PPh_3)]$	0.70	1.6	0.9	2.3
$[Rh(bab)(CO)(PPh_3)]$	0.77	2.0	0.6	4.7
$[Rh(bav)(CO)(PPh_3)]$	0.80	1.7	0.5	4.0

^a At 25 °C.

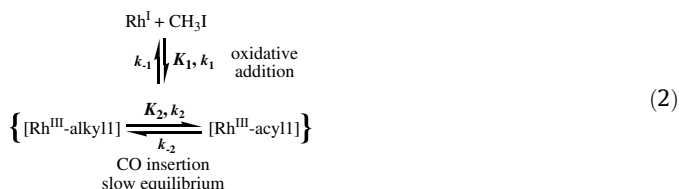
2.2. Kinetics

2.2.1. Infrared study

Kinetic measurements for the reaction of $Rh(bap)(CO)(PPh_3)$ (**7**), $[Rh(bab)(CO)(PPh_3)]$ (**8**) or $[Rh(bav)(CO)(PPh_3)]$ (**9**) with iodomethane in chloroform were first carried out using IR spectroscopy by monitoring the changes in absorbance of peaks at different $\nu(CO)$ bands. This technique is ideal to distinguish between CO bonds in metal–CO complexes that resonate at ~ 1980 – 2000 cm^{-1} for Rh^I -monocarbonylphosphine complexes and at ~ 2050 – 2100 cm^{-1} for Rh^{III} -alkyl complexes and CO bonds in metal–COCH₃ complexes that resonate at ~ 1700 – 1750 cm^{-1} for Rh^{III} -acyl complexes [17]. All three Rh^I complexes followed the same reaction sequence in reaction with iodomethane. Fig. 1 is a representative example, illustrating the infrared spectroscopic observations made during the oxidative addition of iodomethane to $[Rh(bav)(CO)(PPh_3)]$ (**9**), as well as the following carbonyl insertion and deinsertion steps. Fig. 2 gives the absorbance-time data obtained for this reaction.

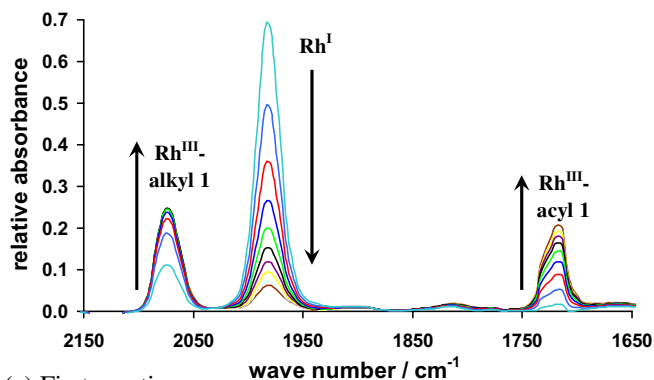
The first step for the reaction between iodomethane and $[Rh(bav)(CO)(PPh_3)]$ (**9**) shows that the disappearance of the Rh^I complex (signal at 1982 cm^{-1} , $k_{obs} = 0.0066(2) s^{-1}$) leads to the immediate formation of a Rh^{III} -alkyl1 species (signal at 2075 cm^{-1} , $k_{obs} = 0.037(1) s^{-1}$) and the simultaneous formation of the Rh^{III} -acyl1 species at a slightly slower rate (signal at 1720 cm^{-1} , $k_{obs} = 0.0033(2) s^{-1}$) as a result of CO insertion. The rate of formation of the Rh^{III} -alkyl1 species at 2075 cm^{-1} is virtually higher than the rate of disappearance of Rh^I due to the fact that Rh^{III} -alkyl1 is simultaneously being converted to Rh^{III} -acyl1 at a rate of $0.0033(2) s^{-1}$. When utilizing the consecutive reaction kinetic model on the time-absorbance data of Rh^{III} -alkyl1, it was found that the Rh^{III} -alkyl1 species appeared at practically the same rate as the Rh^I disappearance, see Section 2.2.2 below. The observed slower rate of Rh^{III} -acyl1 appearance is considered to imply that the equilibrium involving the CO insertion step, is too slow to be maintained during the oxidative addition of iodomethane to Rh^I .

The first reaction that can thus be presented as follow:

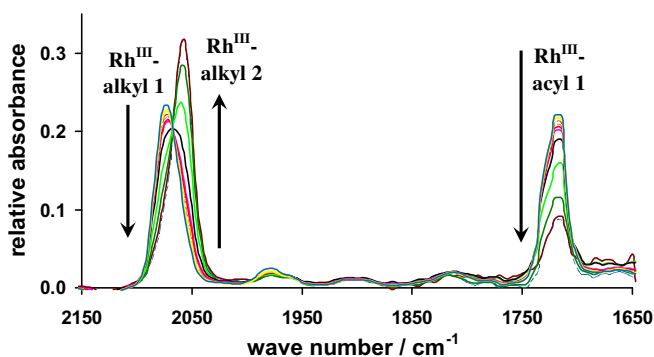


In Eq. (2) above a typical structure of a Rh^{III} -alkyl complex would be $[Rh^{III}(\beta\text{-diketonato})(CH_3)(CO)(PPh_3)(I)]$ while for Rh^{III} -acyl $[Rh^{III}(\beta\text{-diketonato})(COCH_3)(PPh_3)(I)]$ is representative (β -diketonato = bap, bab or bav). Based on infrared measurements, however, it is not possible to offer any structural data on a Rh^{III} -alkyl or a Rh^{III} -acyl.

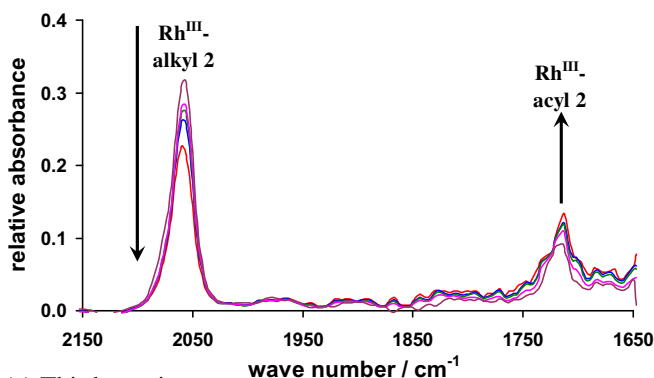
The second reaction set, for the reaction between iodomethane and $[Rh(bav)(CO)(PPh_3)]$ (**9**) in chloroform as observed on the IR, is



(a) First reaction



(b) Second reaction



(c) Third reaction

Fig. 1. Illustration of the oxidative addition reaction between 0.1730 mol dm^{-3} iodomethane and 0.0003 mol dm^{-3} $[Rh(bav)(CO)(PPh_3)]$ (**9**) as monitored on the IR spectrophotometer between 1650 and 2150 cm^{-1} in chloroform at 25 °C. The first reaction is indicated by the disappearance of Rh^I and the simultaneous appearance of Rh^{III} -alkyl1 and Rh^{III} -acyl1. The second reaction is indicated by the simultaneous disappearance of Rh^{III} -alkyl1 and Rh^{III} -acyl1 and the formation of Rh^{III} -alkyl2 species. The third reaction is indicated by the disappearance of Rh^{III} -alkyl2 and the formation of Rh^{III} -acyl2 species.

much slower than the first reaction set ($t_{1/2} \approx 4$ h). During the second reaction set, the Rh^{III} -acyl1 species at 1720 cm^{-1} ($k_{obs} = 0.000049(1) s^{-1}$) and the Rh^{III} -alkyl1 species at 2075 cm^{-1} ($k_{obs} = 0.000053(5) s^{-1}$) disappear as the formation of a new Rh^{III} -alkyl 2 species at 2056 cm^{-1} ($k_{obs} = 0.000052(2) s^{-1}$) occurs. This wavenumber of the new Rh^{III} -alkyl 2 is 19 cm^{-1} lower than the wavenumber of the Rh^{III} -alkyl1. The disappearance of the Rh^{III} -alkyl1 species at 2075 cm^{-1} and the Rh^{III} -acyl1 species at 1720 cm^{-1} at kinetically the same rate, supplies further evidence that there exists an equilibrium between the Rh^{III} -alkyl1 and the Rh^{III} -acyl1 species that is fast enough to be maintained during the formation of the Rh^{III} -alkyl2. This second reaction was found

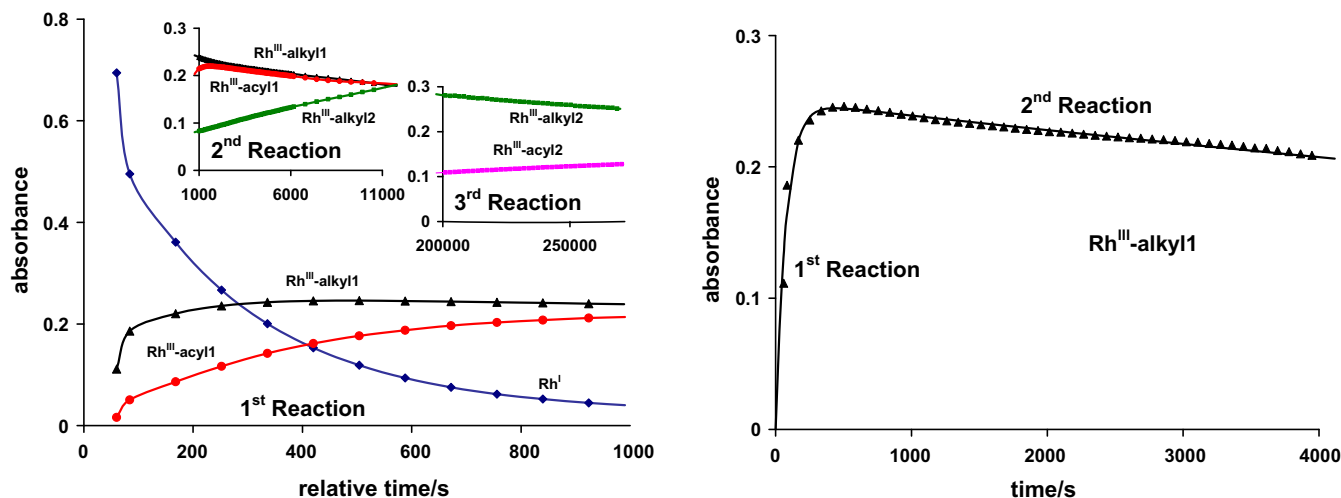
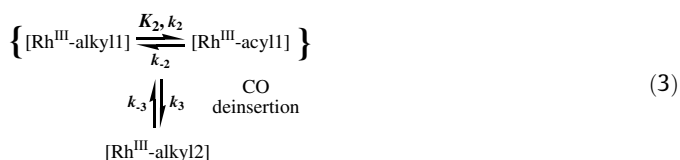


Fig. 2. IR absorbance vs. time data of the reaction between iodomethane ($0.1730 \text{ mol dm}^{-3}$) and $[\text{Rh}(\text{bav})(\text{CO})(\text{PPh}_3)]$ (**9**) ($0.0003 \text{ mol dm}^{-3}$) in chloroform at 25°C . Left: the data obtained for the three reaction sets. Right: the solid line is obtained when experimental kinetic data of $\text{Rh}^{\text{III}}\text{-alkyl1}$ were fitted to the consecutive reaction model of Eq. (14).

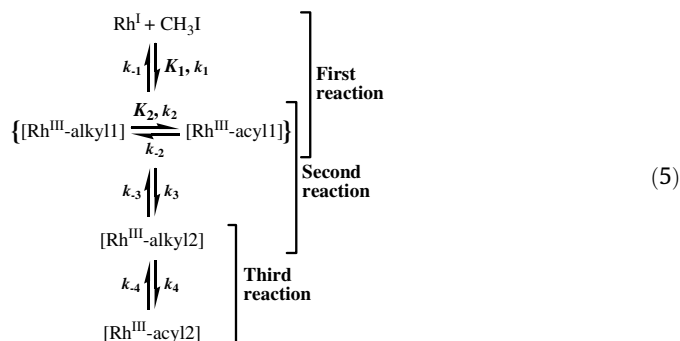
to be first order and independent of $[\text{CH}_3\text{I}]$. The kinetic data of the second reaction are consistent with



The third reaction set for the reaction between iodomethane and $[\text{Rh}(\text{bav})(\text{CO})(\text{PPh}_3)]$ (**9**) in chloroform, as observed on the IR, includes the very slow ($t_{1/2} \approx 38 \text{ h}$) disappearance of the $\text{Rh}^{\text{III}}\text{-alkyl2}$ species at 2059 cm^{-1} ($k_{\text{obs}} = 0.000005(1) \text{ s}^{-1}$) and the appearance of a new $\text{Rh}^{\text{III}}\text{-acyl2}$ species at 1716 cm^{-1} at the same rate. The third reaction set is also first order and $[\text{CH}_3\text{I}]$ independent. The kinetic data of the third reaction are consistent with



The overall reaction sequence for this oxidative addition reaction, obtained by combining Reactions (2)–(4), may therefore be represented as



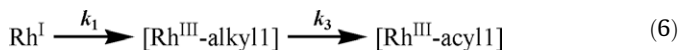
The reaction between iodomethane and $[\text{Rh}(\text{bap})(\text{CO})(\text{PPh}_3)]$ (**7**) or $[\text{Rh}(\text{bab})(\text{CO})(\text{PPh}_3)]$ (**8**) followed the same reaction sequence as described above for the reaction between iodomethane and $[\text{Rh}(\text{bav})(\text{CO})(\text{PPh}_3)]$ (**9**) in chloroform. Table 2 gives a summary of the rate constants determined.

Table 2
Kinetic rate constants for the oxidative addition of iodomethane to $[\text{Rh}(\beta\text{-diketonato})(\text{CO})(\text{PPh}_3)]$ complexes **7**, **8** and **9** in chloroform at 25°C , as monitored by IR spectrophotometry.

Complex	$[\text{CH}_3\text{I}]/\text{mol dm}^{-3}$	Rh ^I disappearance		Rh ^{III} -alkyl1 formation		Rh ^{III} -acyl1 formation	
		$k_{\text{obs}} (\text{s}^{-1})$	$k_1 (\text{dm}^3 \text{mol}^{-1} \text{s}^{-1})$	$k_{\text{obs}} (\text{s}^{-1})$	$k_{\text{obs}} (\text{s}^{-1})$	$k_{\text{obs}} (\text{s}^{-1})$	$k_{\text{obs}} (\text{s}^{-1})$
<i>First reaction</i>							
$[\text{Rh}(\text{bap})(\text{CO})(\text{PPh}_3)]$	0.2085	0.0071(4)	0.034(1)	0.036(5)	0.0049(1)		
$[\text{Rh}(\text{bab})(\text{CO})(\text{PPh}_3)]$	0.1500	0.0071(2)	0.047(2)	0.0152(1)	0.0042(3)		
$[\text{Rh}(\text{bav})(\text{CO})(\text{PPh}_3)]$	0.2143	0.0066(2)	0.031(2)	0.037(1)	0.0033(2)		
		Rh ^{III} -alkyl1 disappearance		Rh ^{III} -acyl1 disappearance		Rh ^{III} -alkyl2 formation	
		$k_{\text{obs}} (\text{s}^{-1})$	$k_{\text{obs}} (\text{s}^{-1})$	$k_{\text{obs}} (\text{s}^{-1})$	$k_{\text{obs}} (\text{s}^{-1})$	$k_{\text{obs}} (\text{s}^{-1})$	$k_{\text{obs}} (\text{s}^{-1})$
<i>Second reaction</i>							
$[\text{Rh}(\text{bap})(\text{CO})(\text{PPh}_3)]$	0.00033(3)		0.00037(8)		0.00041(10)		
$[\text{Rh}(\text{bab})(\text{CO})(\text{PPh}_3)]$	0.00106(1)		0.00089(2)		0.00113(1)		
$[\text{Rh}(\text{bav})(\text{CO})(\text{PPh}_3)]$	0.000053(5)		0.000049(1)		0.000052(2)		
		Rh ^{III} -acyl2 formation		Rh ^{III} -alkyl2 disappearance			
		$k_{\text{obs}} (\text{s}^{-1})$	$k_{\text{obs}} (\text{s}^{-1})$	$k_{\text{obs}} (\text{s}^{-1})$	$k_{\text{obs}} (\text{s}^{-1})$		
<i>Third reaction</i>							
$[\text{Rh}(\text{bap})(\text{CO})(\text{PPh}_3)]$		0.00015(2)			0.00013(2)		
$[\text{Rh}(\text{bab})(\text{CO})(\text{PPh}_3)]$		0.000005(2)			0.000006(1)		
$[\text{Rh}(\text{bav})(\text{CO})(\text{PPh}_3)]$		0.000005(2)			0.000005(1)		

2.2.2. Consecutive reaction treatment

If k_{-1} and k_{-2} are very small in Reaction (5) and if the equilibrium K_2 was found to be fast enough to be maintained during the formation of Rh^{III} -alkyl2, then the first two steps in Reaction (5) can be approximated by



In this case, the formation and depletion of the Rh^{III} -alkyl1 can be studied by using the consecutive reaction treatment in Eq. (13). Upon performing a least squares fit of the available IR absorbance vs. time data of the Rh^{III} -alkyl1 peak for the reaction in chloroform to Eq. (13) (graph shown for Rh^{III} (bav)-alkyl1 in Fig. 2, right) the rate constants were determined as $k_{1\text{obs}} = 0.0128(6) \text{ s}^{-1}$ ($k_1 = 0.0597 \text{ dm}^3 \text{ mol}^{-1} \text{ s}^{-1}$) and $k_3 = 0.000047(5) \text{ s}^{-1}$. The value of $k_{1\text{obs}}$ corresponds kinetically close with the value obtained for the disappearance of the Rh^{I} from data treatment utilizing Eq. (12), $k_1 = 0.031(2) \text{ dm}^3 \text{ mol}^{-1} \text{ s}^{-1}$. The value of k_3 , utilizing Eq. (13), was practically the same as the value of $0.000049(1) \text{ s}^{-1}$ which was determined by treating the depletion of the Rh^{III} -alkyl1 during the second reaction in isolation (Eq. (12)).

2.2.3. UV/Vis study

The reaction between iodomethane and $[\text{Rh}(\text{bap})(\text{CO})(\text{PPh}_3)]$ (7), $[\text{Rh}(\text{bab})(\text{CO})(\text{PPh}_3)]$ (8) or $[\text{Rh}(\text{bav})(\text{CO})(\text{PPh}_3)]$ (9) was also monitored on a UV/Vis spectrophotometer and all three reaction steps could be uniquely identified for each complex. The reaction rate constant obtained for the first step corresponded to the rate constant for the disappearance of the Rh^{I} species as observed on the IR. The rate constant for the second and third steps also corresponded to the rate constant for the second and third reaction sets as observed on the IR spectrophotometer. The second step is the formation of the Rh^{III} -alkyl2 species and the third step is the formation of the final reaction product, the Rh^{III} -acyl2 species.

The temperature and iodomethane concentration dependence of the oxidative addition (first) reaction step as given by Reaction (2) is illustrated in Fig. 3 for $[\text{Rh}(\text{bap})(\text{CO})(\text{PPh}_3)]$ (7), $[\text{Rh}(\text{bab})(\text{CO})(\text{PPh}_3)]$ (8) and $[\text{Rh}(\text{bav})(\text{CO})(\text{PPh}_3)]$ (9). Plots of k_{obs} vs. $[\text{CH}_3\text{I}]$ are linear with non zero intercepts (Fig. 3), indicating the oxidative addition reactions to be first order in iodomethane and hence second order overall. This linear dependence on concentration of iodomethane is characteristic of oxidative addition to d^8 transition-metal complexes [19]. The non zero intercept implies that the k_{-1} step in Reaction (5) exists. The rate constants and the activation parameters, which were obtained from the temperature dependence study utilizing Eq. (14), are summarized in Table 3. The large negative values obtained for the first step for ΔS^\ddagger are consistent with an interpretation that the transition state for the forward step 1 reaction occurs via an associative mechanism, where the coordination number changes from 4 to 6.

2.2.4. ^1H and ^{31}P NMR study

The reaction between iodomethane and the rhodium(I) complexes of this study was also monitored by ^1H and ^{31}P NMR in order to obtain additional insight into this reaction. NMR spectroscopy is an excellent technique for the identification of the different isomers resulting from the oxidative addition reaction of $[\text{Rh}(\beta\text{-diketonato})(\text{CO})(\text{PPh}_3)]$ with iodomethane. On the ^1H NMR, Rh^{III} -alkyl complexes of the type of $[\text{Rh}(\beta\text{-diketonato})(\text{CH}_3)(\text{CO})(\text{PPh}_3)(\text{I})]$ can be identified by the resonance signal of the CH_3 -group at ca 1.4–1.7 ppm. This signal is a doublet of doublets due to coupling of the H with Rh (spin 1/2) and P (spin 1/2). Rh^{III} -acyl complexes of the type of $[\text{Rh}(\beta\text{-diketonato})(\text{COCH}_3)(\text{PPh}_3)(\text{I})]$ can be identified by the sharp resonance signal of the acyl COCH_3 -group at ca 3 ppm [20]. The ^{31}P NMR of the rhodium complexes gives a doublet with $J(^{31}\text{P}\text{-}^{103}\text{Rh}) = \text{ca } 170 \text{ ppm}$ for Rh^{I} complexes, ca 120 ppm for Rh^{III} -

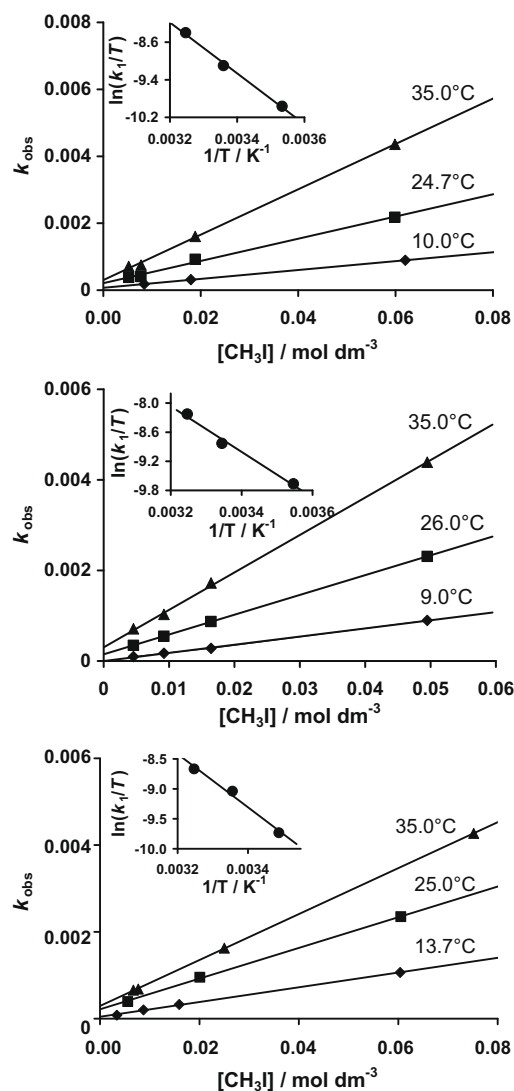
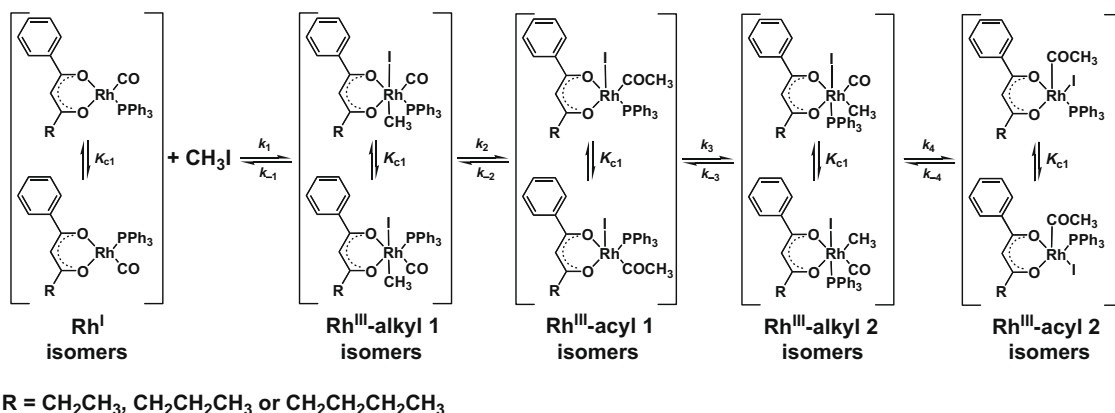


Fig. 3. Temperature and iodomethane concentration dependence for the oxidative addition of iodomethane to $[\text{Rh}(\text{bap})(\text{CO})(\text{PPh}_3)]$ (7) (top), $[\text{Rh}(\text{bab})(\text{CO})(\text{PPh}_3)]$ (8) (middle) and $[\text{Rh}(\text{bav})(\text{CO})(\text{PPh}_3)]$ (9) (bottom) as monitored on the UV/Vis spectrophotometer in chloroform at 340 nm for the first reaction $\{\text{Rh}^{\text{I}} + \text{CH}_3\text{I} = [\text{Rh}^{\text{III}}\text{-alkyl1} = \text{Rh}^{\text{III}}\text{-acyl1}]\}$ (oxidative addition step). Inset: Linear dependence between $\ln(k_1/T)$ and $1/T$, as predicted by the Eyring equation.

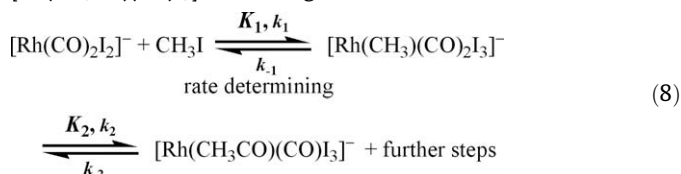
alkyl complexes and ca 150 ppm for Rh^{III} -acyl complexes [18,20,21]. Selected fragments of ^1H and ^{31}P NMR spectra, recorded during the oxidative addition of iodomethane to $[\text{Rh}(\text{bap})(\text{CO})(\text{PPh}_3)]$ (7) in CDCl_3 , are given in Figs. 4 and 5, respectively. The same reaction sequence, as observed on IR and UV/Vis, was observed on the ^1H NMR and the ^{31}P NMR. The new feature introduced by the NMR study, is the existence of two structural isomers for each reaction intermediate in Reaction (5). This is expected, since the Rh^{I} complexes exist of two structural isomers A and B (Scheme 2) which are in a fast equilibrium with each other. The two observed isomers of each intermediate will be referred to as A and B, e.g. Rh^{III} -alkyl1A and Rh^{III} -alkyl1B. The choice of the labels is arbitrary and has no significance, see Figs. 4 and 5. The rate constants, obtained for the A and B structural isomers of a specific reaction intermediate, were within experimental error the same suggesting that a fast equilibrium between the A and B structural isomers exists for each reaction intermediate, according to Reaction (5). Taking into account that two main isomers exist for each



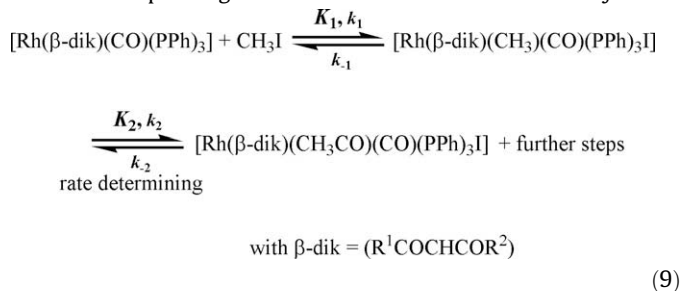
Scheme 3. Mechanism for iodomethane oxidative addition and CO migratory insertion in monocarbonylphosphine complexes of the type $[\text{Rh}(\text{C}_6\text{H}_5)\text{COC}(\text{HCO}(\text{CH}_2)_n\text{CH}_3)(\text{CO})(\text{PPh}_3)]$ indicating the proposed structures of the rhodium(III) reaction intermediates and -products.

2.2.5. Reactivity correlation: iodomethane oxidative addition to $[\text{Rh}(\beta\text{-diketonato})(\text{CO})(\text{PPh}_3)]$ complexes vs. addition to the Monsanto catalyst

The rate-determining step in the rhodium-iodide catalyzed reaction of methanol to acetic acid, is the oxidative addition of iodomethane to $[\text{Rh}(\text{CO})_2\text{I}_2]^-$ to produce the $[\text{Rh}(\text{CH}_3)(\text{CO})_2\text{I}_3]^-$ alkyl reaction intermediate that rapidly converts to an acyl $[\text{Rh}(\text{CH}_3\text{CO})(\text{CO})\text{I}_3]^-$ according to the reaction scheme



The corresponding reaction scheme of the current study is



For all complexes of the type $[\text{Rh}(\text{R}^1\text{COCHCOR}^2)(\text{CO})(\text{PPh}_3)]$ it is clear that a decrease in the group electronegativity of R^1 and R^2 (better electron donating power) leads to an increased reactivity of Rh^I with iodomethane (Table 4), with complexes 7–9 being the most reactive. Complexes 7–9 revealed a second order oxidative addition rate approximately 500–600 times faster than that observed for $[\text{Rh}(\text{CO})_2\text{I}_2]^-$. The rate-determining step for the oxidative addition reaction of 7–9, the carbonyl insertion step, is *ca* 60 times faster than the rate-determining oxidative addition step of iodomethane to $[\text{Rh}(\text{CO})_2\text{I}_2]^-$ [1]. An increase in the size of the alkyl group on the β -diketonato of $[\text{Rh}(\text{C}_6\text{H}_5)\text{COCHCOR}(\text{CO})(\text{PPh}_3)]$, with $\text{R} = (\text{CH}_2)_n\text{CH}_3$, $n = 1\text{--}3$, did not hamper the rate of oxidative addition.

3. Conclusions

The reaction rate of the first oxidative addition step or the following carbonyl insertion and deinsertion steps of $[\text{Rh}(\text{C}_6\text{H}_5)\text{COCHCOR}(\text{CO})(\text{PPh}_3)] + \text{CH}_3\text{I}$ (with $\text{R} = (\text{CH}_2)_n\text{CH}_3$, $n = 1\text{--}3$) in chloroform, were not influenced by the increasing alkyl chain length of the R group on the β -diketonato ligand. However, the electron donating properties of the R chain accelerate the oxidative addition step 500–600 times faster than the rate-determining oxidative addition step of iodomethane to the Monsanto catalyst $[\text{Rh}(\text{CO})_2\text{I}_2]^-$ under similar conditions [1].

Table 4

Kinetic rate constants for the oxidative addition step in chloroform at 25 °C of $[\text{Rh}(\text{R}^1\text{COCHCOR}^2)(\text{CO})(\text{PPh}_3)]$, as well as group electronegativities of the R substituents of the β -diketonato ligand.

Abbreviation of β -diketonato ligand ($\text{R}^1\text{COCHCOR}^2$)	R^1	R^2	$(\chi_{\text{R}1} + \chi_{\text{R}2})/(\text{Gordy scale})^a$	$k_1^f/\text{mol}^{-1} \text{dm}^3 \text{s}^{-1}$	k_2^f/s^{-1}	Ref.
bab	C_6H_5	$\text{CH}_2\text{CH}_2\text{CH}_3$	4.62	0.0437(1)	0.0042(3)	^e
bap	C_6H_5	CH_2CH_3	4.52	0.0333(9)	0.0049(1)	^e
bav	C_6H_5	$\text{CH}_2\text{CH}_2\text{CH}_2\text{CH}_3$	4.43	0.0354(8)	0.0033(2)	^e
dtm	$\text{C}_4\text{H}_9\text{S}$	$\text{C}_4\text{H}_9\text{S}$	4.20	0.029(1)	^f	[21]
bth	$\text{C}_4\text{H}_9\text{S}$	Ph	4.31	0.0265(6)	^f	
acac	CH_3	CH_3	4.68	0.024(3) ^c	0.0065(5)	[8]
dbm	C_6H_5	C_6H_5	4.42	0.00961 ^b	^f	[35]
ba	C_6H_5	CH_3	4.55	0.00930 ^b	–	[31]
fctfa	Fc	CF_3	4.88	0.00611(1)	^f	[10]
tta	CF_3	$\text{C}_4\text{H}_9\text{S}$	5.11	0.00171(4)	^f	[18]
tfaa	CF_3	CH_3	5.35	0.00146 ^b	–	[31]
tfba	C_6H_5	CF_3	5.22	0.00112 ^b	–	[31]
hfaa	CF_3	CF_3	6.02	0.00013(1)	0.00048(9)	[9]
Monsanto catalyst				0.000068 ^d	0.13	[1]

^a Group electronegativities of this study and Ref. [15].

^b Value in acetone.

^c Value in 1,2-dichloroethane.

^d In CH_2Cl_2 at 35 °C.

^e Rate constants from this study.

^f $(k_2)_{\text{obs}} = k_1[\text{CH}_3\text{I}]$ due to fast equilibrium K_2 in Eq. (9).

4. Experimental

4.1. Materials and apparatus

Solid reagents used in preparations (Merck, Aldrich and Fluka) were used without further purification. Liquid reactants and solvents were distilled prior to use; water was doubly distilled. Organic solvents were dried according to published methods [28].

4.2. Synthesis

4.2.1. β -Diketones 1–3

The general procedure to synthesize the phenyl-containing β -diketones Hbap (1-phenylpentane-1,3-dione, propanylacetophenone, $C_6H_5COCH_2COCH_2CH_3$) (**1**); Hbab (1-phenylhexane-1,3-dione, butylacetophenone, $C_6H_5COCH_2COCH_2CH_2CH_3$) (**2**) and Hbav (1-phenylheptane-1,3-dione, valerylacetophenone, $C_6H_5COCH_2COCH_2CH_2CH_2CH_3$) (**3**) was as follows: a Schlenk setup was used. In a three-necked round bottomed flask, with a magnetic stirrer bar, acetophenone (1.2015 g, 10 ml) was added in dried, freshly distilled and degassed THF (1.0 ml). The flask was attached to a gas flow adapter and N_2 bubbler. The solution was degassed while being stirred for 30 min. Lithium diisopropylamide (LDA) (6.0 ml of 1.8 mol dm^{-3} solution in hexane, 10.8 mmol) was added to the solution at 0 °C with a syringe, under nitrogen. A color change to clear orange showed that a slight excess of LDA was added. The solution was allowed to stir for 10 min before an appropriate ester (10 mmol) was slowly added into the solution at 0 °C while stirring. The reaction mixture was stirred overnight under N_2 atmosphere. Ether (30 ml) was added into the reaction mixture and stirred for 20 min. The resulting precipitate was filtered and washed with ether (2 \times 30 ml). Ether (20 ml) was added to the precipitate, and 0.3 M HCl (20 ml) dropped by while stirring till a pH lower than 4 was reached. The product was extracted with ether (2 \times 50 ml). The combined ether extracts were dried with anhydrous $MgSO_4$ and removed by evaporation. Silica gel column chromatography was used to separate the product.

Characterization data for Hbap (1): 1H NMR (δ /ppm, $CDCl_3$): 1.1 (3H, t, keto CH_3), 1.2 (3H, t, enol CH_3), 2.5 (2H, q, enol CH_2), 2.6 (2H, q, keto CH_2), 4.1 (2H, s, keto CH_2), 6.2 (1H, s, enol CH), 7.4–7.9 (5H, m, 2 \times C_6H_5); ^{13}C NMR (δ /ppm, $CDCl_3$): 198.5 (s, $COCH_2CH_3$), 183.4 (COPh), 135.4, 132.6, 129.2, 129.0, 127.4 (s, Ph), 95.9 (s, COCCO), 32.8 (s, CH_2CH_3), 10.1 (s, CH_2CH_3). R_f = 0.39 (ether:hexane = 1: 4). Elemental Anal. Calc. for $C_{11}H_{11}O_2$: C, 75.41; H, 6.33. Found: C, 75.23; H, 6.31%.

Characterization data for Hbab (2): 1H NMR (δ /ppm, $CDCl_3$): 0.9 (3H, t, keto CH_3), 1.0 (3H, t, enol CH_3), 1.6 (2H, q, keto CH_2), 1.7 (2H, q, enol CH_2), 2.4 (2H, t, enol CH_2), 2.6 (2H, t, keto CH_2), 4.1 (2H, s, keto CH_2), 6.2 (1H, s, enol CH), 7.5–8.0 (5H, m, 2 \times C_6H_5); ^{13}C NMR (δ /ppm, $CDCl_3$): 197.1 (s, $COCH_2CH_2CH_3$), 179.0 (COPh), 135.5, 133.6, 129.2, 129.0, 127.4 (s, Ph), 96.6 (s, COCCO), 41.5 (s, $CH_2CH_2CH_3$), 19.7 (s, $CH_2CH_2CH_3$), 14.2 (s, $CH_2CH_2CH_3$). R_f = 0.34 (ether:hexane = 1:4). Elemental Anal. Calc. for $C_{12}H_{13}O_2$: C, 76.17; H, 6.92. Found: C, 76.05; H, 6.85%.

Characterization data for Hbav (3): 1H NMR (δ /ppm, $CDCl_3$): 0.9 (3H, t, keto CH_3), 1.0 (3H, t, enol CH_3), 1.3 (2H, m, keto CH_2), 1.4 (2H, m, enol CH_2), 1.6 (2H, m, keto CH_2), 1.7 (2H, m, enol CH_2), 2.4 (2H, t, enol CH_2), 2.6 (2H, t, keto CH_2), 4.1 (2H, s, keto CH_2), 6.2 (1H, s, enol CH), 7.5–8.0 (5H, m, 2 \times C_6H_5); C NMR (δ /ppm, $CDCl_3$): 197.1 (s, $COCH_2CH_2CH_2CH_3$), 183.4 (COPh), 135.5, 132.4, 129.0, 129.2, 127.4 (s, Ph), 96.5 (s, COCCO), 39.3 (s, $CH_2CH_2CH_2CH_3$), 28.3 (s, $CH_2CH_2CH_2CH_3$), 22.2 (s, $CH_2CH_2CH_2CH_3$), 14.1 (s, $CH_2CH_2CH_2CH_3$). R_f = 0.58 (ether:hexane = 1:4). Elemental Anal. Calc. for $C_{13}H_{15}O_2$: C, 76.82; H, 7.44. Found: C, 76.83; H, 7.45%.

4.2.2. $[Rh(\beta\text{-diketonato})(CO)_2]$ complexes 4–6

The general procedure was as follows: $[Rh_2Cl_2(CO)_4]$ was prepared *in situ* by refluxing $RhCl_3 \cdot 3H_2O$ (0.1001 g, 0.38 mmol) in DMF (3 ml) until the color changed from red to yellow (ca 30 min) [29]. The dimer-containing solution was allowed to cool on ice and an equivalent amount of solid β -diketone (0.38 mmol) was slowly added while stirring. After 30 min of stirring at room temperature, the crude product $[Rh(\beta\text{-diketonato})(CO)_2]$, for complex $[Rh(bap)(CO)_2]$ (**4**), was precipitated with an excess of water, extracted with ether, washed with water, dried with $MgSO_4$ and solvent removed under reduced pressure. Recrystallization was done with hot hexane. The crude product $[Rh(\beta\text{-diketonato})(CO)_2]$, for complexes $[Rh(bab)(CO)_2]$ (**5**) and $[Rh(bav)(CO)_2]$ (**6**), was precipitated with an excess of water, filtered, air dried and recrystallized with hot hexane.

$[Rh(bap)(CO)_2]$ (4**):** Yield: 0.0899 g, 27%. M.p. 79–81 °C. IR (cm^{-1}) = 2065 and 2008. 1H NMR (δ /ppm, $CDCl_3$): 1.2 (3H, t, CH_3), 2.4 (2H, q, CH_2), 6.2 (1H, s, CH) 7.4–7.9 (5H, m, C_2H_5). Elemental Anal. Calc. for $RhC_{13}H_{11}O_4$: C, 46.7; H, 3.3. Found: C, 46.6; H, 3.1%.

$[Rh(bab)(CO)_2]$ (5**):** Yield: 0.0615 g, 17%. M.p. 53–55 °C. IR (cm^{-1}) = 2084 and 2014. 1H NMR (δ /ppm, $CDCl_3$): 1.0 (3H, t, CH_3), 1.7 (2H, m, CH_2), 2.4 (2H, t, CH_2), 6.3 (1H, s, CH), 7.4–7.9 (5H, m, C_2H_5). Elemental Anal. Calc. for $RhC_{14}H_{13}O_4$: C, 48.3; H, 3.8. Found: C, 48.2; H, 3.7%.

$[Rh(bav)(CO)_2]$ (6**):** Yield: 0.0657 g, 18%. M.p. 45–50 °C. 1H NMR (δ /ppm, $CDCl_3$) 0.9 (3H, t, CH_3), 1.4 (2H, m, CH_2), 1.7 (2H, m, CH_2), 2.4 (2H, t, CH_2), 6.3 (1H, s, CH), 7.4–7.9 (5H, m, C_2H_5). Elemental Anal. Calc. for $RhC_{15}H_{15}O_4$: C, 49.7; H, 4.2. Found: C, 49.5; H, 4.0%.

4.2.3. $[Rh(\beta\text{-diketonato})(CO)(PPh_3)]$ complexes 7–9

The general procedure was as follows: to a solution of $[Rh(\beta\text{-diketonato})(CO)_2]$ (0.2 mmol) in hot *n*-hexane (3 cm^3) PPh_3 (0.2 mmol) was added. The resulting reaction mixture was stirred for ca 1 min, until no more CO gas was released, and filtered. Silica gel column chromatography was used to purify the product where necessary. Crystallographic pure crystals of the desired complexes $[Rh(bap)(CO)(PPh_3)]$ (**7**), $[Rh(bab)(CO)(PPh_3)]$ (**8**) and $[Rh(bav)(CO)(PPh_3)]$ (**9**), were obtained after recrystallization from acetone.

$[Rh(bap)(CO)(PPh_3)]$ (7**):** Yield: 0.0955 g, 16%. M.p. 139–144 °C. IR (cm^{-1}) = 1982. 1H NMR (δ /ppm, $CDCl_3$) isomer A: 1.2 (3H, t, CH_3), 2.5 (2H, q, CH_2), 6.2 (1H, s, CH), 7.0–8.0 (20H, m, aromatic); isomer B: 0.6 (3H, t, CH_3), 2.0 (2H, q, CH_2), 6.1 (1H, s, CH), 7.0–8.0 (20H, m, aromatic); ratio isomer A: isomer B = 1.00: 0.69. ^{31}P NMR (δ /ppm, $CDCl_3$) isomer A: 48.88 ($^1J(^{31}P\text{--}^{103}Rh)$ = 176 Hz) isomer B: 48.36 ($^1J(^{31}P\text{--}^{103}Rh)$ = 177 Hz). Elemental Anal. Calc. for $RhC_{30}PH_{26}O_3$: C, 63.4; H, 4.6. Found: C, 63.5; H, 4.5%.

$[Rh(bab)(CO)(PPh_3)]$ (8**):** Yield: 0.0732 g, 13%. M.p. 135–138 °C. IR (cm^{-1}) = 1981. 1H NMR (δ /ppm, $CDCl_3$) isomer A: 1.0 (3H, t, CH_3), 1.8 (2H, m, CH_2), 2.5 (2H, t, CH_2), 6.2 (1H, s, CH), 7.0–8.0 (20H, m, aromatic); isomer B: 0.6 (3H, t, CH_3), 1.2 (2H, m, CH_2), 2.0 (2H, t, CH_2), 6.1 (1H, s, CH), 7.0–8.0 (20H, m, aromatic); ratio isomer A: isomer B = 1.00: 0.78. ^{31}P NMR (δ /ppm, $CDCl_3$) isomer A: 48.80 ($^1J(^{31}P\text{--}^{103}Rh)$ = 175 Hz) isomer B: 48.56 ($^1J(^{31}P\text{--}^{103}Rh)$ = 175 Hz). Elemental Anal. Calc. for $RhC_{31}PH_{28}O_3$: C, 63.9; H, 4.8. Found: C, 63.8; H, 4.6%.

$[Rh(bav)(CO)(PPh_3)]$ (9**):** Yield: 0.0805 g, 14%. M.p. 139–145 °C. IR (cm^{-1}) = 1983. 1H NMR (δ /ppm, $CDCl_3$) isomer A: 1.0 (3H, t, CH_3), 1.4 (2H, m, CH_2), 1.7 (2H, m, CH_2), 2.5 (2H, t, CH_2), 6.2 (1H, s, CH), 7.0–8.0 (20H, m, aromatic); isomer B: 0.7 (3H, t, CH_3), 1.2 (4H, m, 2 \times CH_2), 2.0 (2H, t, CH_2), 6.1 (1H, s, CH), 7.0–8.0 (20H, m, aromatic); ratio isomer A: isomer B = 1.00: 0.78. ^{31}P NMR (δ /ppm, $CDCl_3$) isomer A: 48.84 ($^1J(^{31}P\text{--}^{103}Rh)$ = 176 Hz) isomer B: 48.53 ($^1J(^{31}P\text{--}^{103}Rh)$ = 175 Hz). Elemental Anal. Calc. for $RhC_{32}PH_{30}O_3$: C, 64.4; H, 5.1. Found: C, 64.2; H, 5.1%.

4.3. Spectroscopy and spectrophotometry

NMR measurements at 25 °C were recorded on a Bruker Advance II 600 NMR spectrometer [¹H (600.130 MHz) and ³¹P (242.937 MHz)]. The chemical shifts were reported relative to SiMe₄ (0.00 ppm) for the ¹H spectra and relative to 85% H₃PO₄ (0 ppm) for the ³¹P spectra. Positive values indicate downfield shift. IR spectra were recorded from neat samples on a Digilab FTS 2000 infrared spectrophotometer. UV/Vis spectra were recorded on a Cary 50 Probe UV/Vis spectrophotometer.

4.4. Acid dissociation constant (*K_a*) determinations

The p*K_a* values were determined by measuring the absorbance of 0.07 mmol dm⁻³ β-diketone solutions at different pH's during an acid–base titration in acetonitrile:water mixtures, 1:9 by volume, μ = 0.100 mol dm⁻³ (NaClO₄) at 25.0(5) °C as described previously [30].

4.5. Kinetic measurements

Oxidative addition reactions were monitored on the IR (by monitoring formation and disappearance of the carbonyl peaks), on the UV/Vis (by monitoring the change in absorbance at the indicated wavelength) spectrophotometers and on the NMR (by monitoring the change in integration units of the specified signals) spectrometer. All kinetic measurements were monitored under pseudo-first-order conditions with [CH₃I] 10–400 times the concentration of the [Rh(β-diketonato)(CO)(PPh₃)] complex in the specified solution. The concentration [Rh(β-diketonato)(CO)(PPh₃)] ≈ 0.0003 mol dm⁻³ for UV/Vis measurements, ≈0.03 mol dm⁻³ for IR measurements and ≈0.03 mol dm⁻³ for NMR measurements. Kinetic measurements, under pseudo-first-order conditions for different concentrations of [Rh(β-diketonato)(CO)(PPh₃)] at a constant [CH₃I], confirmed that the concentration of [Rh(β-diketonato)(CO)(PPh₃)] did not influence the value of the observed kinetic rate constant. The observed first-order rate constants were obtained from least-square fits of absorbance (IR and UV/Vis) or integration units (NMR) vs. time data [31].

The [Rh(β-diketonato)(CO)(PPh₃)] complexes **7**, **8** and **9** were tested for stability in chloroform by means of overlay IR and UV/Vis spectra for at least 24 h. A ¹H NMR spectrum of complexes **7**, **8** and **9**, after 48 h in solution of CDCl₃, confirmed stability in solution.

4.6. Calculations

4.6.1. Calculations of % keto isomer and *K_c* value of the β-diketones

The % keto tautomer and equilibrium constant, *K_c* applicable to Scheme 1, were obtained from

$$\% \text{ keto tautomer} = \frac{(I \text{ of keto signal})}{\{(I \text{ of keto signal}) + (I \text{ of enol signal})\}} \times 100\% \quad (10)$$

with *I* = integral value of 1H.

$$K_c = \frac{(\% \text{ enol tautomer})}{(\% \text{ keto tautomer})} = \frac{(100 - \% \text{ keto tautomer})}{(\% \text{ keto tautomer})} \quad (11)$$

4.6.2. Calculation of kinetic rate constants and activation parameters

Pseudo-first-order rate constants, *k_{obs}*, were calculated by fitting [27] kinetic data to the first-order equation [32]

$$[A]_t = [A]_0 e^{-k_{\text{obs}}t} \quad (12)$$

with [A]_t and [A]₀ = the concentration of the indicated species at time *t* and at *t* = 0 (UV/Vis or IR experiments) or integral values for the specified peaks on NMR spectra. The experimentally determined pseudo first order rate constants were converted to second

order rate constants, *k₁*, by determining the slope of the linear plots of *k_{obs}* against the concentration of the incoming iodomethane ligand. Non-zero intercepts implied that *k_{obs}* = *k₁*[CH₃I] + *k₋₁* and that the *k₋₁* step in the proposed reaction mechanism exists.

Kinetic data for the consecutive reaction treatment [28] of IR data applicable to the general reaction Rh^I $\xrightarrow{k_1}$ Rh^{II}-alkyl1 $\xrightarrow{k_2}$ Rh^{II}-alkyl2 were fitted to Eq. (12) when monitoring the disappearance of Rh^I and to Eq. (13) for monitoring the appearance and disappearance of Rh^{III}-alkyl1.

$$[\text{Rh}^{\text{III}} - \text{alkyl1}]_t = \frac{k_{1\text{obs}}[\text{Rh}^{\text{I}}]_0}{k_3 - k_{1\text{obs}}} [\exp(-k_{1\text{obs}}t) - \exp(-k_3t)] \quad (13)$$

All kinetic mathematical fits were done utilizing the fitting program MINSQ [27]. The error of all the data is presented according to crystallographic conventions, for example *k_{obs}* = 0.0236(1) s⁻¹ implies *k_{obs}* = (0.0236 ± 0.0001) s⁻¹.

The activation parameters were determined from the Eyring relationship [28],

$$\ln \frac{k}{T} = -\frac{\Delta H^\ddagger}{RT} + \frac{\Delta S^\ddagger}{R} + \ln \frac{k_B}{h} \quad (14)$$

with Δ*H*[‡] = activation enthalpy, Δ*S*[‡] = activation entropy, *k* = rate constant, *k_B* = Boltzmann's constant, *T* = temperature, *h* = Planck's constant, *R* = universal gas constant and the activation free energy Δ*G*[‡] = Δ*H*[‡] – *T*Δ*S*[‡].

4.6.3. Calculation of thermodynamic quantities

The reaction enthalpy, Δ_r*H* [33,34], for the equilibrium shown in Scheme 2 is calculated by the van't Hoff equation

$$\ln K_{c(\text{ii})} = \ln K_{c(\text{i})} - \frac{\Delta_r H}{R} \left(\frac{1}{T_{(\text{ii})}} - \frac{1}{T_{(\text{i})}} \right) \quad (15)$$

where ln *K_{c(ii)}* and ln *K_{c(i)}* are the equilibrium constants at temperatures *T_(ii)* and *T_(i)*, *R* = 8.314 J K⁻¹ mol⁻¹. The thermodynamic quantity “Gibbs free energy”, Δ_r*G*, and reaction entropy, Δ_r*S*, can be calculated from the equations Δ_r*G* = – *RT* ln *K_c* and Δ_r*G* = Δ_r*H* – *T*Δ_r*S* [30].

Acknowledgements

Financial assistance by the South African National Research Foundation under Grant number 2067416 and the Central Research Fund of the University of the Free State is gratefully acknowledged.

Appendix A. Supplementary material

Supplementary data associated with this article can be found, in the online version, at doi:10.1016/j.jorganchem.2008.10.040.

References

- [1] P.M. Maitlis, A. Haynes, G.J. Sunley, M.J. Howard, J. Chem. Soc., Dalton Trans. (1996) 2187.
- [2] J.D. Atwood, Coord. Chem. Rev. 83 (1988) 93.
- [3] C. Masters, Homogeneous Transition-Metal Catalysis: A Gentle Art, Chapman & Hall, London, 1981.
- [4] M.G. Pedrós, A.M. Masdeu-Bultó, J. Bayardon, D. Sinou, Catal. Lett. 107 (2006) 205.
- [5] V.C. Gibson, S.K. Spitzmesser, Chem. Rev. 103 (2003) 283.
- [6] L. Gonslavi, H. Adams, G.J. Sunley, E. Ditzel, A. Haynes, J. Am. Chem. Soc. 124 (2002) 13597.
- [7] E.A. Shor, A.M. Shor, V.A. Nasluzov, A.I. Rubaylo, J. Struct. Chem. 46 (2005) 220.
- [8] S.S. Basson, J.G. Leipoldt, A. Roodt, J.A. Venter, T.J. van der Walt, Inorg. Chim. Acta 119 (1986) 35.
- [9] S.S. Basson, J.G. Leipoldt, J.T. Nel, Inorg. Chim. Acta 84 (1984) 167.
- [10] J. Conradie, G.J. Lamprecht, A. Roodt, J.C. Swarts, Polyhedron 23 (2007) 5075–5087.

- [11] R. Ugo, A. Pasini, A. Fusi, S. Cerini, *J. Am. Chem. Soc.* 944 (1972) 7364.
- [12] M.C. Etter, D.A. Jahn, Z. Yrbanczyk-Lipkowska, *Acta Crystalllogr., Sect. C: Cryst. Struct. Commun.* 260 (1987) 43.
- [13] G.J. van Zyl, G.J. Lamprecht, J.G. Leipold, *Inorg. Chim. Acta* 143 (1988) 223.
- [14] W.C. du Plessis, T.G. Vosloo, J.C. Swarts, *J. Chem. Soc., Dalton Trans.* (1998) 2507.
- [15] W.C. du Plessis, J.C. Erasmus, G.J. Lamprecht, J. Conradie, T.S. Cameron, M.A.S. Aquino, J.C. Swarts, *Can. J. Chem.* 77 (1999) 378.
- [16] A.A. Grinberg, *Acta Physiochim. USSR* 3 (1935) 573.
- [17] J. Conradie, G.J. Lamprecht, S. Otto, J.C. Swarts, *Inorg. Chim. Acta* 328 (2002) 191.
- [18] M.M. Conradie, J. Conradie, *Inorg. Chim. Acta* 361 (2008) 208.
- [19] A.J. Hart-Davis, W.A.G. Graham, *Inorg. Chem.* 9 (1970) 2658.
- [20] Yu.S. Varshavsky, T.G. Cherkasova, N.A. Buzina, L.S. Bresler, *J. Organomet. Chem.* 464 (1994) 239.
- [21] M.M. Conradie, J. Conradie, *Inorg. Chim. Acta* 361 (2008) 2285.
- [22] M. Conradie, J. Conradie, *Inorg. Chim. Acta*, in press. doi: 10.1016/j.ica.2008.04.046.
- [23] M. Conradie, J. Conradie, *S. Afr. J. Chem.* 61 (2008) 102.
- [24] J.A. Cabeza, V. Riera, M.A. Villa-Garcia, L. Ouahab, S. Triki, *J. Organomet. Chem.* 41 (1992) 323.
- [25] C.H. Cheng, B.D. Spivack, R. Eisenberg, *J. Am. Chem. Soc.* 99 (1977) 3003.
- [26] L.J. Damoense, W. Purcell, A. Roodt, *Rhodium Ex.* 14 (1995) 4.
- [27] A. Roodt, G.J.J. Steyn, *Recent Res. Devel. Inorg. Chem.* 2 (2000) 1.
- [28] B.S. Furniss, A.J. Hannaford, P.W.G. Smith, A.R. Tatchell, in: *Vogel's Textbook of Practical Organic Chemistry*, fifth ed., John Wiley & Sons, New York, 1994, p. 409.
- [29] (a) Y.S. Varshavskii, T.G. Cherkasova, *Russ. J. Inorg. Chem.* 12 (1967) 899; (b) A. Rusina, A.A. Vıcek, *Nature* 206 (1965) 295 (London).
- [30] W.C. du Plessis, T.G. Vosloo, J.C. Swarts, *J. Chem. Soc., Dalton Trans.* (1998) 2507.
- [31] L. Helm, MINSQ, Non-linear Parameter Estimation and Model Development, Least Squares Parameter Optimization V3.12, MicroMath Scientific Software, Salt Lake City, UT, 1990.
- [32] J.H. Espenson, in: *Chemical Kinetics and Reaction Mechanisms*, 2nd ed., McGraw-Hill, New York, 1995, pp. 15, 49, 70–75.
- [33] S.H. Maron, J.B. Maron, in: *Fundamentals of Physical Chemistry*, Macmillan Publishing Co. Inc., New York, 1974, pp. 376–383.
- [34] P.W. Atkins, in: *Physical Chemistry*, fifth ed., Oxford University Press, Oxford, 1994, pp. 141–154, 276, 288–289.
- [35] D. Lamprecht, Ph. D. Thesis, University of the Orange Free State, R.S.A., 1998.